American Journal of Modern Physics
2017; 6(6): 132-139
http://www.sciencepublishinggroup.com/j/ajmp
doi: 10.11648/j.ajmp.20170606.14
ISSN: 2326-8867 (Print); ISSN: 2326-8891 (Online)

Synthesis, Structural, Electrical and Thermal Properties of $ScFeO_3$ Ceramic

Falguni Bhadala, Vikash Kumar Jha, Lokesh Suthar, Maheshwar Roy*

Department of Physics, Mohanlal Sukhadia University, Udaipur, Rajasthan, India

Email address:

fbhadala@gmail.com (F. Bhadala), vkjha1988@yahoo.com (V. K. Jha), lokesh_17292@yahoo.com (L. Suthar), mroy1959@yahoo.co.in (M. Roy)

*Corresponding author

To cite this article:

Falguni Bhadala, Vikash Kumar Jha, Lokesh Suthar, Maheshwar Roy. Synthesis, Structural, Electrical and Thermal Properties of $ScFeO_3$ Ceramic. *American Journal of Modern Physics*. Vol. 6, No. 6, 2017, pp. 132-139. doi: 10.11648/j.ajmp.20170606.14

Received: August 12, 2017; **Accepted**: August 28, 2017; **Published**: September 25, 2017

Abstract: The ceramic sample of $ScFeO_3$ (SFO) has been prepared by standard high temperature solid state reaction method using high purity oxides. The formation of the compound as well as structural analysis has been carried out by X-ray diffraction method which confirmed the rhombohedral symmetry with polar space group R3c. The average grain size obtained by the Scherrer formula is of the order of 560 Å. The surface morphology of SFO has been investigated by Atomic Force Microscopy (AFM). The average roughness obtained by two dimensional surface morphology ranges from 5.80 nm to 20.2 nm for surface area $5\times5\mu m^2$ to $10\times10\mu m^2$ respectively. The dielectric constant and dielectric loss as a function of frequency (100Hz-1MHz) and temperature (RT-650K) have been measured. At RT and 1kHz frequency the material shows high dielectric constant value (around 1800) with lossy nature. The transport properties such as I-V characteristics, ac and dc conductivities have been measured and activation energy was calculated using the Arrhenius relation. The I-V characteristic along with ac and dc conductivity studies show semiconducting behaviour with dc activation energy of 0.81eV. The Magnetic measurement indicates weak ferromagnetic behaviour. The Enthalpy change (ΔH), Specific heat (C_p) and % Weight-loss of the compound have been measured using DTA/TGA technique. The DTA curve shows transition around 1088K with C_p =2.3$Jg^{-1}K^{-1}$ and ΔH=18.4Jg^{-1}. The low weight loss (around 2%) from RT -1200K suggest that the material is thermally stable. The results are discussed in detail.

Keywords: X-ray Diffraction, Dielectric, Conductivity, Activation Energy, Enthalpy Change, Specific Heat

1. Introduction

The surge of interest in multiferroic materials over the past fifteen years has been driven by their fascinating physical properties and huge potential for technological applications [1]. The attempts to combine more than one ferroic orders like ferroelectric, ferromagnetic, ferroelastic, etc. in one system started in 1960's, by two groups i.e., one group of Smolenskii in St. Peterburg [2] and the other by Venevtsev in Moscow [3]. Multiferroics can be classified into two groups according to their origin of coexisting magnetic and ferroelectric orders. Type I multiferroics are those in which magnetic and ferroelectric orders arise independent of each other, for example, $BiFeO_3$ [4] while in type II multiferroics, magnetic order can induce ferroelectric order and vice-versa which suggests that there lies a strong coupling between these two orders, for example, $RMnO_3$ (where R is rare earth element) [5].

Most of the promising multiferroic materials are those which consist of transition metal perovskites [6]. Scandium Ferrite, $ScFeO_3$ (SFO) is one such ferrite that has been synthesised under high pressure (15 GPa) and low temperature (above 110K) [7]. The high pressure phase exhibits a polar R3c space group with highly distorted ScO_6 and FeO_6 octahedra. SFO has high magnetic ordering at 545K owing to G-type antiferromagnetic order of the Fe^{+3} atoms [8]. It is interesting to note that in a perovskite with formula ABO_3, the ferroelectric B site cation requires empty d-orbitals while the ferromagnetism requires B-site

cations with partially filled d-orbitals. Since both these conditions cannot be met simultaneously in a material therefore to overcome these difficulty, perovskite oxides with small A-site cation has been synthesised to create polar magnetic materials [9]. The stability and distortions of perovskites are interpreted using Goldschmidt tolerance factor $t = \frac{r_A + r_O}{\sqrt{2}(r_B + r_O)}$ where r_A, r_B, r_O are the ionic radii of the cation A, cation B and Oxygen anion [10-11]. The perovskite structure is stable when $0.77 < t < 0.99$; if r_A and r_B are ionic radii based on octahedral co-ordination and r_O = 1.4Å [12]. For SFO, t= 0.742 which implies that A-site cation is much smaller than B-type cation and hence the SFO is less stable and more distorted perovskite structure [12]. Due to small A-site cation in SFO the $a^-a^-a^-$ tilt pattern in Glazer notation [13] is electrostatically and energetically unstable as A site is severely under bonded [14]. Thus in SFO A-site undergoes ferroelectric distortion while B-site is magnetic. Therefore, SFO is classified as type-I multiferroic [14]. From the literature survey it is observed that a lot of work have been reported on multiferroic $BiFeO_3$ and other materials but no much work have been reported on SFO due to its peculiar behaviour at the same time it has been synthesized at high pressure and low temperature and hence present paper reports on synthesis of SFO at high temperature and normal pressure and its other physical properties.

2. Experimental

2.1. Sample Preparation

The ceramic sample of $ScFeO_3$ was prepared in laboratory by high temperature solid state reaction method using stoichiometric proportions of high purity precursors: Sc_2O_3 and Fe_2O_3 by the following chemical reaction.

$$\mathbf{Sc_2O_3 + Fe_2O_3 \rightarrow 2\,ScFeO_3} \quad (1)$$

These ingredients were thoroughly mixed by grinding for 2 hours in wet medium (acetone) in agate mortar. The calcinations of the above mixture were carried out at high temperature (1473K) for 12 hrs. The calcined powder was than compacted by hydraulic press at pressure 5 tons/cm^2 to form pellets of thickness 2.01 mm and diameter of 10.50 mm. The sintering of pellet was carried at 1623K for 6 hrs.

2.2. Characterization

The formation of the compound was confirmed by X-ray diffraction using Rigaku Mini Flex Ultima-IV X-ray Diffractometer with Cuk_α radiation of wavelength λ= 1.54 Å in a wide range of Bragg's angle 30º≤ 2θ ≤70º at a scanning rate of 5 degree/min. The Grain size was calculated using the Scherrer formula [15].

$$\mathbf{D = \frac{K\lambda}{\beta \cos\theta}} \quad (2)$$

Where λ is the wavelength of source radiation, K is the Scherrer constant having numerical value 0.94, β is the full width at half maxima (FWHM) and θ is the Bragg angle.

Strain (ε) was calculated using the formula [16].

$$\boldsymbol{\varepsilon = \frac{\beta}{4\tan\theta}} \quad (3)$$

Also the dislocation density which is defined as the length of dislocation lines per unit volume of the crystal was calculated using the Williamson-Smallman relation [17] i.e.,

$$\boldsymbol{\delta = \frac{1}{D^2}} \quad (4)$$

Where δ is the dislocation density and D is the grain size of the sample under study.

The number of crystallites per unit area (N) was calculated using formula [18]

$$\mathbf{N = \frac{t}{D^3}} \quad (5)$$

Where t is the thickness of the pellet and D is the grain size.

The three dimensional microstructure and surface morphology was analysed using Atomic Force Microscopy (model NT-MDT SOLVER NEXT, Moscow, Russia) at RT. The Dielectric constant (ε'), Dissipation factor (ε'') and ac conductivity were measured at 100Hz, 1KHz, 10KHz, 100KHz and 1MHz as a function of temperature from RT to 773K in air atmosphere using HIOKI 3532-50 LCR Hi-Tester. The I-V characteristic of the SFO was studied using an Agilent B2901A Electrometer. The dc conductivity was measured from room temperature to 773K using a laboratory made set up in accordance with Ohm's Law. The magnetization measurement was carried out using vibrating sample magnetometer (VSM) model (No.7304) at room temperature up to the applied field of 1 Tesla. The specific heat, enthalpy change and % weight loss of the compound were measured as a function of temperature from 303K to 1173K in heating and cooling cycles at a scanning rate of 20K /min using Perkin-Elmer STA-6000 (DTA/TGA) thermal analyser in inert atmosphere.

3. Results and Discussion

3.1. Structural Properties

3.1.1. XRD Analysis

The X-Ray Diffraction pattern of SFO is shown in figure 1. The XRD pattern (Figure 1) revealed the rhombohedral symmetry [5] using the hexagonal setting. The observed X-ray data coincided well with the ICSD DATA file (262384). The observed values of inter-planar spacing's, intensities, FWHM and particle sizes are shown in table 1. The calculated surface parameters such as grain size, dislocation density, strain etc. are shown in table 2.

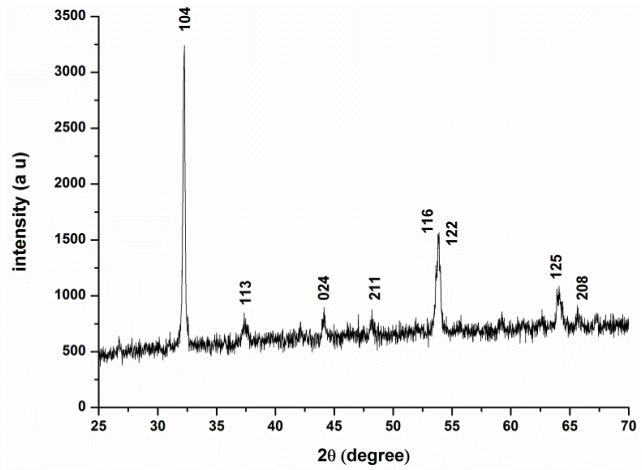

Figure 1. *XRD pattern of SFO at RT.*

Table 1. *Detailed structural parameters of SFO.*

2θ	h k l	d_{obs}	I_{obs}	I_{obs}/I_0	β= FWHM	GRAIN SIZE(Å)
32.2	104	2.777	100	1	0.166	519
37.34	113	2.406	5	0.051	0.5	175
44.13	024	2.050	6	0.062	0.22	406
48.06	211	1.892	4	0.038	0.29	315
53.64	116	1.707	15	0.148	0.14	654
53.87	122	1.701	32	0.322	0.19	495
63.9	125	1.456	12	0.116	0.29	332
64.34	208	1.447	6	0.058	0.06	1580

Table 2. *Calculated values of surface parameters.*

AVERAGE GRAIN SIZE (D)	560Å (by Scherrer formula)
DISLOCATION DENSITY (δ)	1080.077 μm^{-2}
STRAIN (ε)	0.0024
NO. OF CRYSTALLITES PER UNIT AREA (N)	97536579.91 μm^{-2}

3.1.2. Surface Morphology

The three dimensional surface morphology of SFO at RT was analyzed using AFM. The SFO sample was scanned with scanning area of 5×5 μm^2 and 10×10 μm^2 and semi-contact scanning mode was used to analyse the sample which are shown in figure 2(a, b).

The three dimensional surface morphological image with the scanned area 5×5 μm^2 (figure 2a) shows a very peculiar behaviour and looks like a sea conch with series of transverse patches on its surface. When the scanning area increased from 5×5 μm^2 to 10×10 μm^2 (figure 2b), the three dimensional morphology differs from the previous one. Here the half part of the conch like shape is the same but the side and lower parts show spreading with spike like hills and vallies. The conch like surface with patchy pattern may be caused due to high temperature sintering of the material which has created strain on the surface.

To see the surface behaviour in two dimension using the same instrument we have scanned the same areas as earlier and are shown in figure 3(a, b). The two dimensional surface images figure 3a and 3b show wavy patch like pattern with dark and bright portion representing vallies and hills in different domain regions on the surface which also confirmed that the surface of the sample is strained.

For scanning area 5×5 μm^2, the dark patches represent the valley in height range 0-50 nm while the light patches represent the hills in height range 50-100 nm. The minimum Grain height is 8.11 nm, max. Grain size is 1.53 μm and average roughness of SFO sample in the sampling area (5×5 μm^2) is 5.80 nm.

For scanning area 10×10 μm^2, the dark patches represent the valley in height range 0-150 nm while the light patches represent the hills in height range 50-300 nm. The minimum Grain height is 31.28 nm and the maximum Grain size is 4.59 μm and average roughness of SFO sample in the sampling area (10×10 μm^2) is 20.20 nm.

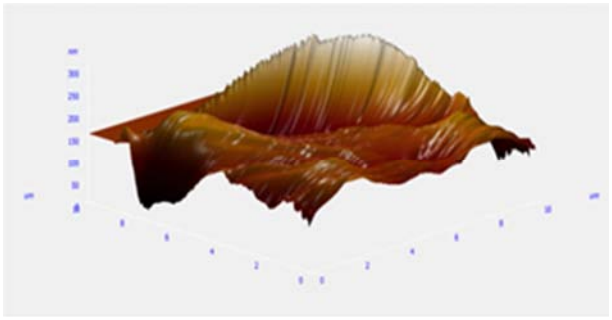

(a)

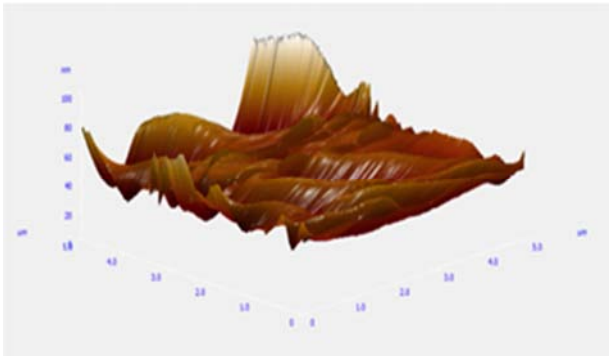

(b)

Figure 2. *3-D surface morphological images of SFO (a) Scan size 5×5 μm^2 (b) Scan size 10×10 μm^2.*

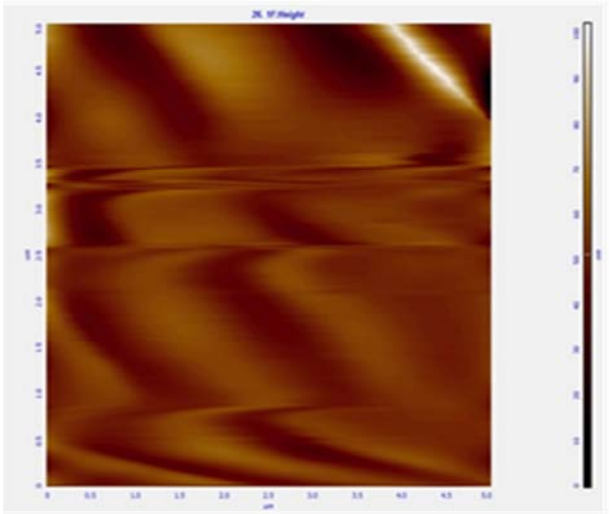

(a)

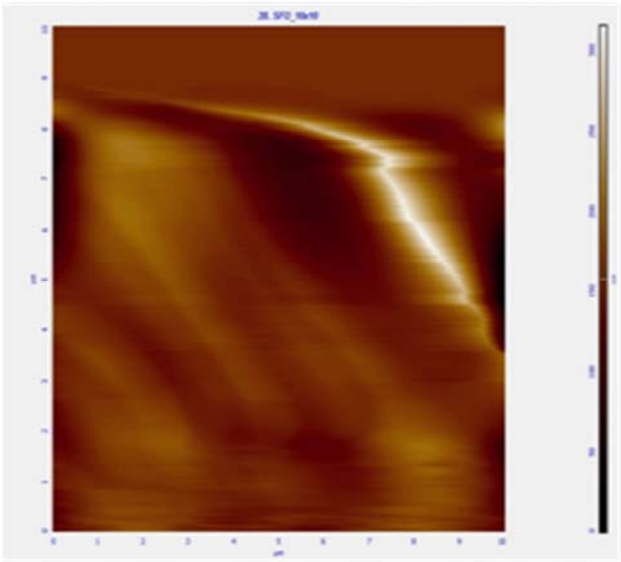

(b)

Figure 3. *2-D surface morphological images of SFO (a) Scan size 5×5 μm² and (b) Scan size 10×10 μm².*

3.2. Dielectric Properties

The Behaviour of dielectric constant with frequency from 100Hz to 5MHz was investigated at room temperature and is shown in figure 4. With the change in frequency dielectric constant also changes due to various polarization processes such as dipolar, interfacial, ionic, electronic etc. which occurs in a material in different frequency range [19]. At lower frequencies dielectric constant has high value which can be explained as a result of space charge polarization due to accumulation of charges at the interface of material [20]. As the frequency increases, dipoles are not able to align themselves with applied electric field. Thus contribution from various other polarization ceases and only electronic polarization contributes to the dielectric constant; as a result dielectric constant decreases with increase in frequency. Further increase of frequency makes no change in dielectric constant and it remains almost constant at higher and higher frequencies.

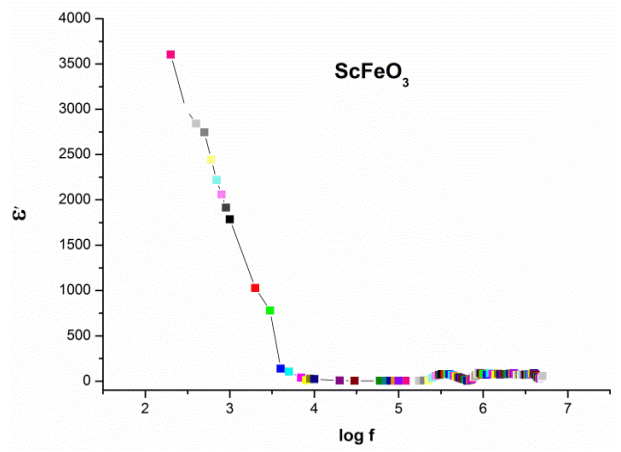

Figure 4. *Variation of Dielectric constant (ε') with frequency at RT.*

The behaviour of Dielectric constant with temperature at frequencies of 10KHz, 100KHz and 1MHz is shown in figure 5. From figure 5, it is observed that the dielectric constant increases with increase of temperature and attains a maximum value around 473K in all cases and then decreases again. In the case of 100KHz frequency the dielectric constant increases abruptly beyond the temperature of 525 K whereas at frequencies of 10KHz and 1MHz, the dielectric constant decreases slowly after the maximum value and then starts increasing again beyond 600K. As discussed earlier this behaviour of dielectric constant may be explained on the basis of different polarization mechanism.

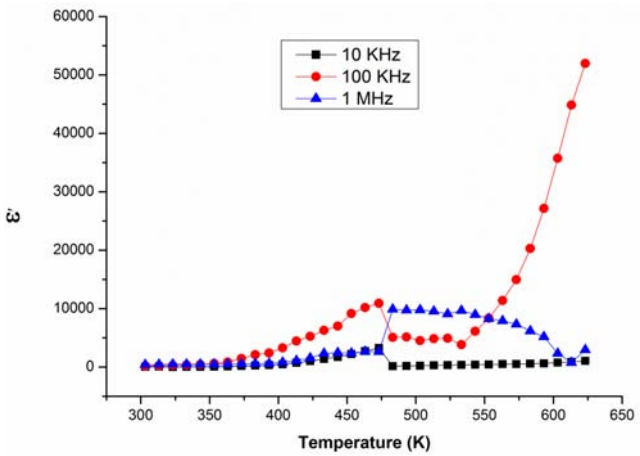

Figure 5. *Variation of Dielectric constant (ε') with Temperature at different frequencies.*

The dissipation factor (ε") vs. temperature curve is shown in figure 6. The dissipation factor is a measure of the dielectric losses in an electrically insulated solid when used in an alternating electric field where the energy is dissipated in the form of heat. Here (figure 6) the dissipation factor shows the same trend as that of dielectric constant with temperature. As the frequency increases, dissipation factor decreases indicating low ac dielectric losses at higher frequency [21]. Thus with the increase in frequency the atomic/ionic and electronic contribution becomes dominant and space charge contribution gradually diminishes resulting in decrease of dissipation factor with increase in frequency [22].

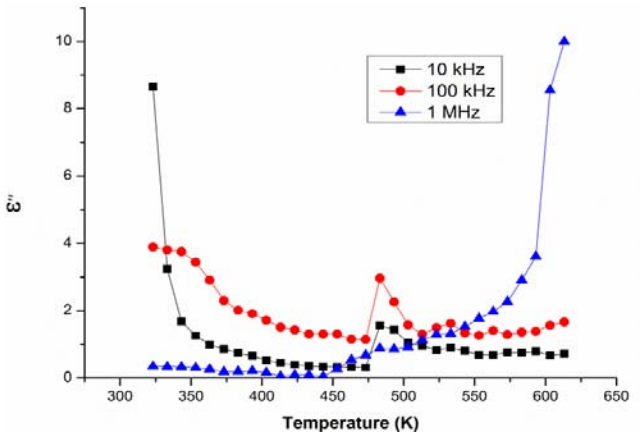

Figure 6. *Variation of dissipation factor (ε") with Temperature.*

3.3. Transport Properties

3.3.1. I-V Characteristics

The current-voltage (I-V) characteristic of SFO is shown in figure 7. From the figure it is observed that the I-V characteristic is non-linear which confirmed the non-linear behaviour of the multiferroic material. Secondly, the I-V characteristic in the first quadrant resembles with that of a ordinary/Zener diode characteristic in the forward bias condition while in the reverse condition the curve does not show the breakdown region like that of Zener diode up to the negative voltage of -1.0 V. For further confirmation the same I-V characteristics has been drawn with reverse polarity. This time the nature of the curve get reversed. This indicates that in one way it behaves like a dc capacitor at the same time it also behaves like a diode. Thus I-V characteristics confirmed the multifunctional behaviour of SFO.

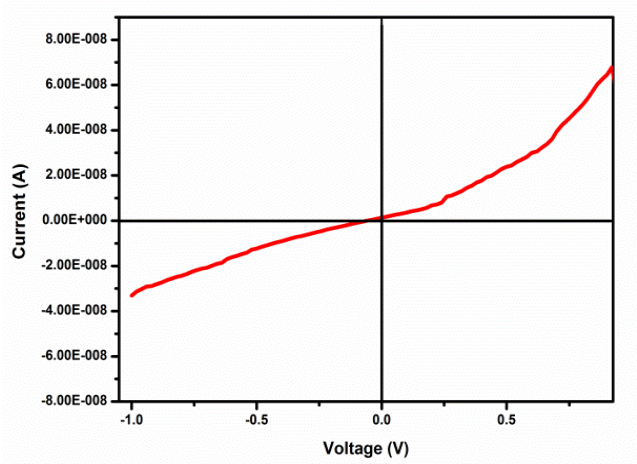

(a)

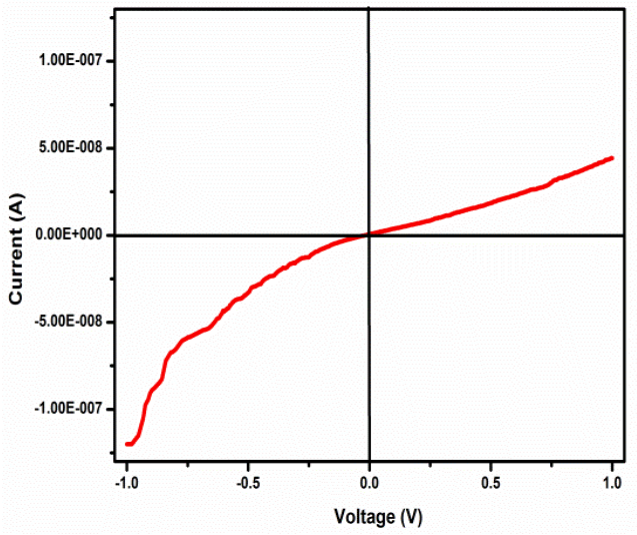

(b)

Figure 7. *I-V characteristics (a) in normal polarity (b) in reverse polarity.*

3.3.2. ac Conductivity

The ac conductivity of SFO was calculated using the formula [22]:

$$\sigma_{ac} = \omega\varepsilon_0\varepsilon'' \quad (6)$$

where, ω = angular frequency = 2лf, where f is the linear frequency

ε_0 = permittivity of free space

ε" = dissipation factor

The variation of log σ_{ac} with respect to 1000/T (K^{-1}) at different frequencies is shown in figure 8.

From the figure it is observed that the conductivity shows a broad hump around the same temperature in all frequencies. This indicates that conductivity is a thermally activated process. Furthermore, from the analysis of ac conductivity as a function of temperature and frequency, the temperature activated electronic transport process has been attributed to large polaronic hopping in the system [23].

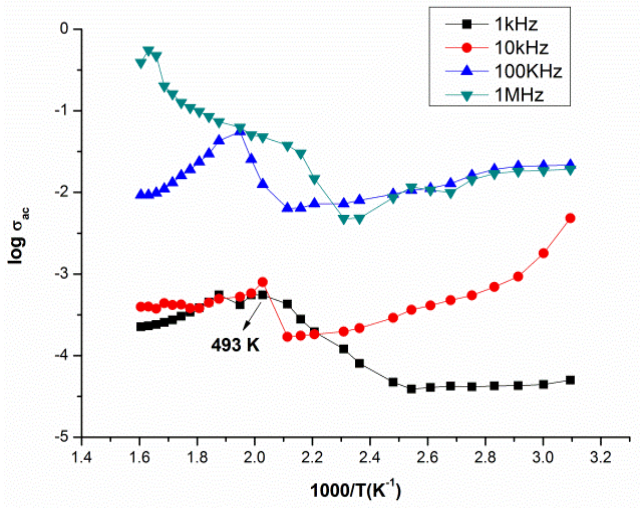

Figure 8. *The log σ_{ac} vs $10^3/T$ curves at different frequencies.*

At 1kHz the ac conductivity increases with increase in temperature and shows a broad hump around 493K. On further increase in frequency from 1kHz to 10kHz, the initial value of conductivity is more but at higher temperature the behaviour is almost same. Further increase of frequency from 10kHz to 100kHz and from 100kHz to 1MHz the conductivity increases more. The values of activation energy in different temperature range at different frequencies are shown in table 3.

Table 3. *Shows the calculated values of activation energy in different temperature range at different specified frequencies.*

TEMPERATURE (K) ⇨	300-350	350-400	400-450	450-500	500-600
FREQUENCY ⇩	ACTIVATION ENERGY (eV)				
1 kHz	-0.04	0.27	0.51	0.28	-0.28
10 kHz	-0.77	-0.19	1.72	-0.27	-0.083
100 kHz	-0.11	___	___	1.11	-0.43
1 MHz	-0.02	-0.31	0.97	0.60	0.48

3.3.3. dc Conductivity

We have also plotted the log σ_{dc} vs. $10^3/T$ (K^{-1}) curve (figure 9). The curve shows a step like behaviour similar to

that of quantum Hall effect in semiconductor. The curve was fitted linearly and its activation energy was calculated using Arrehinus relation [24]:

$$\sigma = \sigma_o \exp \frac{-Ea}{KT} \quad (7)$$

Where σ = conductivity in Ω^{-1} m^{-1}
σ_0= parameter depending on the material
E_a = activation energy in eV
K = Boltzmann constant = 8.617*10^{-5} eV/K
T = temperature in Kelvin

Activation energy was estimated by the slope of the curve (figure 9) and was found to be 0.81 eV. Thus value of activation energy of $ScFeO_3$ which is less than 1eV refers to ferroelectric semiconducting region which may be possibly caused due to presence of singly ionized oxygen vacancies in the conduction process. From the dc conductivity studies it is observed that the material shows semiconducting ferroelectric behaviour as observed in the case of SbSI and other ferroelectric semiconductor ($BaTiO_3$) [25]. The electrical conduction in solids can also be explained using the energy band model employing the appropriate scattering mechanism. The conduction due to impurities, defects etc. takes place either through band mechanism or through hopping of the thermally activated drift mobility of charge carriers among impurity centres. Thus variation of dc conductivity of SFO material as a function of temperature can be explained on the basis of thermally activated charge carriers [24].

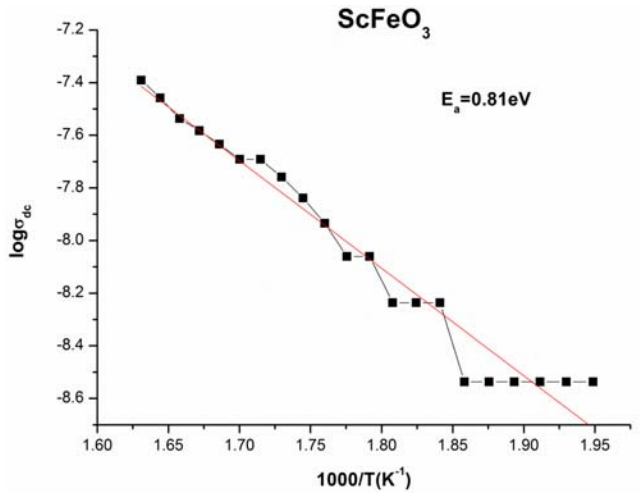

Figure 9. *Variation of dc conductivity ($log\sigma_{dc}$) as a function of inverse temperature.*

3.4. Magnetic Properties

The room temperature magnetization (M) versus field (H) curve is shown in figure 10. The M versus H curve does not show any evidence of saturation. The highest magnetization value of 0.000403 emu/gm at a field of 10 kG, a coercivity (H_c) of 402G and a remanence (M_r) of 0.000049 emu/gm indicates that SFO is a soft magnetic material. The unsaturated loop even at a field of 1T indicates the disordering of ScO_6 and FeO_6 octahedra and G-type anti-ferromagnetic ordering of Fe^{+3} atom exhibiting the polar space group R3c.

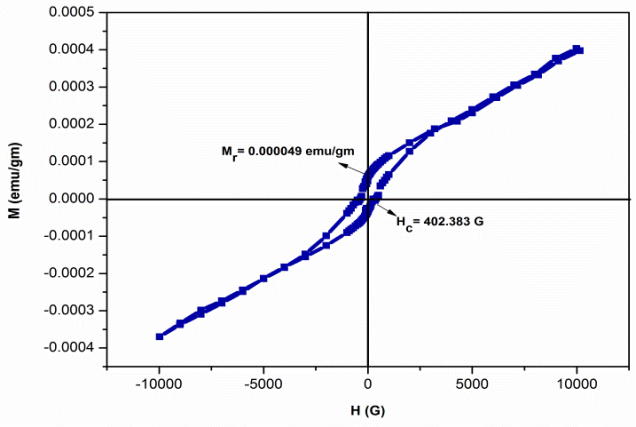

Figure 10. *M-H hysteresis loop at RT.*

3.5. Thermal Properties

The heat flow vs. temperature curve of SFO is shown in figure 11. During heating cycle a small endothermic peak was observed at temperature of 1087K while an exothermic peak was observed at temperature of 1088K in the cooling process. Thus the enthalpy change ΔH and the specific heat capacity at constant pressure was calculated and found to be 18.4Jg^{-1} and 2.3$Jg^{-1}K^{-1}$ respectively. It is based on the first law of thermodynamics which expresses the principle of conservation of energy i.e., when heat is absorbed by a system under specified conditions such as constant pressure, the heat energy of that system changes [26].

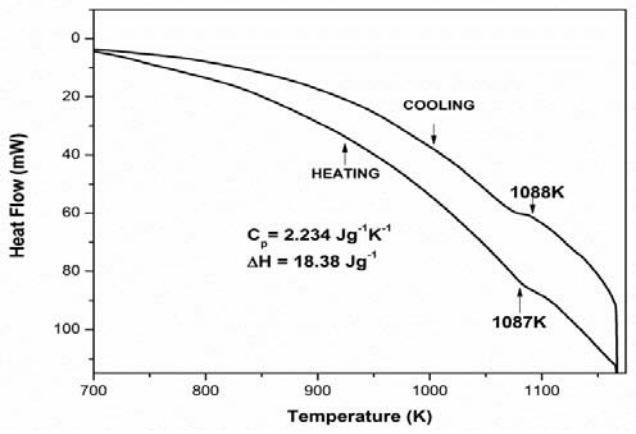

Figure 11. *Heat flow versus temperature curve.*

The amount of heat absorbed by the material in the temperature range 1062K to 1108K was calculated using the equation

$$Q = m \int_{T1}^{T2} c(T)\, dT \quad (8)$$

and it was found to be 165.99 mJ (where m is the mass of the material in mg and c (T) is the specific heat). Also the % weight loss was observed in temperature range 463K to 1163K (figure 12). The very low value of % weight loss

(around 2%) in the specified temperature range suggests that the material is highly stable at high temperature. The high thermal stability of the material is the useful characteristics for device applications.

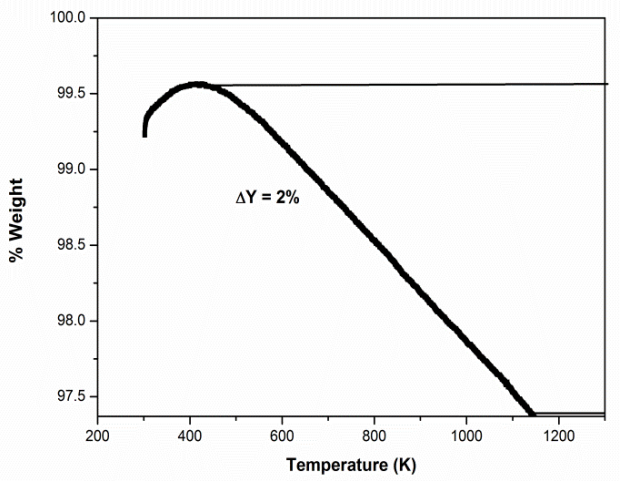

Figure 12. *% Weight loss vs Temperature curve.*

4. Conclusion

The ceramic sample of SFO was prepared by solid state reaction method at high temperature and normal pressure. The structural property was analysed using X-Ray Diffraction. The results revealed that the sample has rhombohedral symmetry with space group R3c. Also surface morphology was analyzed using AFM which revealed that the sample has minimum surface roughness. The dielectric properties indicate that the material has the high value of dielectric constant with lossy nature. The dc conductivity of SFO increases with increase in temperature which imparts that the material exhibit negative temperature coefficient of resistance showing the semiconducting behaviour also supported by the I-V characteristics. The magnetization measurement shows soft magnetic behaviour. The thermal analysis indicates the moderate value of enthalpy change and specific heat with low weight loss even at high temperature (up to 1173K). The high dielectric constant and high thermal stability makes the material suitable for technical applications.

Acknowledgements

Authors are thankful to Dr. N. Lakshmi, Dr. S. Kumar and Dr. M. S. Dhaka in getting the X-Ray Diffraction, VSM, AFM images and I-V characteristics. Also two authors Vikash Kumar Jha and Lokesh Suthar are thankful to UGC for providing the UGC-BSR fellowship.

References

[1] M. M. Vopson, "Fundamentals of multiferroic materials and their possible applications", Critical Reviews in Solid State and Materials Sciences 40(4), 223-250 (2015).

[2] G. A. Smolenskii et al., Segnetoelectrics and Antisegnetoelectrics (Nauka Publishers, Leningrad, 1971) (in Russian); G. A. Smolenskii and I. E. Chupis, Sov. Phys. 25, 475-493 (1982).

[3] Y. N. Venevtsev and V. V. Gagulin, "Search, design and investigation of seignettomagnetic oxides." *Ferroelectrics* 162, 23-31 (1994).

[4] J. Wang, J. B. Neaton, H. Zheng, V. Nagarajan, S. B. Ogale, B. Liu, D. Viehland, V. Vaithyanathan, D. G. Schlom, U. V. Waghmare and N. A. Spaldin, "Epitaxial $BiFeO_3$ multiferroic thin film heterostructures" Science 299(5613), 1719-1722 (2003).

[5] T. Kimura, T. Goto, H. Shintani, K. Ishizaka, T. Arima and Y. Tokura, "Magnetic control of ferroelectric polarization" Letters to Nature 426, 55-58 (2003).

[6] M. Johnsson and P. Lemmens, "Crystallography and chemistry of perovskites", Handbook of magnetism and advanced magnetic materials, John Wiley and Sons, Inc. USA (2007).

[7] T. Kawamoto, K. Fujita, I. Yamada, T. Matoba, S. J. Kim, P. Gao and A. J. Studer, "Room-temperature polar ferromagnet $ScFeO_3$ transformed from a high-pressure orthorhombic perovskite phase", Journal of the American Chemical Society 136(43), 15291-15299 (2014).

[8] S W Lovesey and D D Khalyavin,"Electronic and Magnetic properties of Multiferroic $ScFeO_3$", J. Phys Condens Matter. 14 August 2017, DOI: 10.1088/1361-648X/aa860f.

[9] Y. Hamasaki, T. Shimizu, S. Yasui, T. Taniyama, O. Sakata, and M. Itoh "Crystal Isomers of $ScFeO_3$, *Crystal Growth & Design"* 16(9), 5214-5222 (2016).

[10] V. M. Goldschmidt, "Die gesetze der krystallochemie", Naturwissenschaften. 14(21), 477-485 (1926).

[11] A. A. Belik and W. Yi," High-pressure synthesis, crystal chemistry and physics of perovskites with small cations at the A site", Journal of Physics: Condensed Matter 26(16), 163201(1-13) (2014).

[12] K. Fujita, T. Kawamoto, I. Yamada, O. Hernandez, N. Hayashi, H. Akamatsu and A. J. Studer,"$LiNbO_3$-type $InFeO_3$: Room-Temperature Polar Magnet without Second-Order Jahn–Teller Active Ions", *Chemistry of Materials 28*(18), 6644-6655 (2016).

[13] R. E. Eitel, C. A. Randall, T. R. Shrout, P. W. Rehrig, W. Hackenberger, and S. E. Park, "New high temperature morphotropic phase boundary piezoelectrics based on Bi (Me) O_3–$PbTiO_3$ ceramics", Japanese Journal of Applied Physics 40(10R), 5999-6002 (2001).

[14] A. M. Glazer, "Simple ways of determining perovskite structures", Acta Crystallographica Section A: Crystal Physics, Diffraction, Theoretical and General Crystallography 31(6), 756-762 (1975).

[15] S. M. Patange, S. E. Shirsath, B. G. Toksha, S. S. Jadhav and K. M. Jadhav, "Electrical and magnetic properties of Cr 3+ substituted nanocrystalline nickel ferrite", Journal of Applied Physics 106(2), 023914(1-7) (2009).

[16] S. Lalitha, R. Sathyamoorthy, S. Senthilarasu, A. Subbarayan, and K. Natarajan, "Characterization of CdTe thin film—dependence of structural and optical properties on temperature and thickness", Solar energy materials and solar cells 82(1), 187-199 (2004).

[17] S. Chander, and M. S. Dhaka, “Influence of thickness on physical properties of vacuum evaporated polycrystalline CdTe thin films for solar cell applications”, Physica E: Low-dimensional Systems and Nanostructures 76, 52-59 (2016).

[18] M. Dhanam, R. R. Prabhu, and P. K. Manoj, “Investigations on chemical bath deposited cadmium selenide thin films”, Materials chemistry and Physics 107(2), 289-296 (2008).

[19] M. Roy, S. Jangid, S. K. Barbar, and P. Dave,” Electrical and magnetic properties of $BiFeO_3$ multiferroic ceramics”, Journal of Magnetics 14, 62-65 (2009).

[20] G. Giovannetti, D. Puggioni, P. Barone, S. Picozzi, J. M. Rondinelli and M. Capone, “Magnetoelectric coupling in the type-I multiferroic $ScFeO_3$”, Physical Review B. 94(19), 195116(1-6) (2016).

[21] S. Jangid, S. K. Barbar, I. Bala, And M. Roy, “Structural, thermal, electrical and magnetic properties of pure and 50% La doped $BiFeO_3$ ceramics”, Physica-B. 40, 3694-3699 (2012).

[22] M. Roy and S. Sahu. “Synthesis, electrical and thermal properties of $Bi_4V_{2-x}Zr_xO_{11}$ (x= 0.0, 0.02, 0.06 and 0.10) ceramics” Journal of Electrocermaics. 31, 291-297, (2013).

[23] C. R. Mariappan, G. Govindaraj, S. V. Rathan and G. V. Prakash, “Preparation, characterization, ac conductivity and permittivity studies on vitreous $M_4AlCdP_3O_{12}$ (M= Li, Na, K) system”, Materials Science and Engineering: B. 121(1), 2-8 (2005).

[24] J. Rout, B. N. Parida, P. R. Das and P. Choudhary, “Structural, Dielectric and Electrical Properties of $BiFeWO_6$ Ceramic”, Journal of electronic materials 43(3), 732-739 (2014).

[25] Helen D. Megaw, "Origin of ferroelectricity in barium titanate and other perovskite-type crystals." Acta Crystallographica 5, 739-749 (1952).

[26] M. Roy, I. Bala and S. K. Barbar, “Synthesis, Structural, Electrical and Thermal properties of Ti-doped $Bi_2Sn_2O_7$ pyrochlore”, J. Therm. Anal. Calorim. 110, 559-565 (2012).